^{4}He$(\pi, \pi' p)^3$H reaction near the P_{33} π-nucleon resonance

M. K. Jones,* D. Dehnhard, S. K. Nanda,† and S. M. Sterbenz‡
University of Minnesota, Minneapolis, Minnesota 55455

C. L. Morris and M. Plum
Los Alamos National Laboratory, Los Alamos, New Mexico 87545

J. D. Zumbro‡
University of Pennsylvania, Philadelphia, Pennsylvania 19104
and Los Alamos National Laboratory, Los Alamos, New Mexico 87545

Ahmed H. Hussein
King Fahd University of Petroleum and Minerals, Dhahran 31261 Saudi Arabia

D. S. Oakley,§ M. J. Smithson, A. L. Williams,** J. McDonald, M. A. Bryan, A. H. Fuentes, M. Lynker, D. Crockett, M. A. Machuca, S. Mordechai,†† and C. Fred Moore
University of Texas at Austin, Austin, Texas 78712
(Received 4 March 1992)

Inclusive and exclusive spectra of the ^{4}He$(\pi, \pi' p)$ reaction were measured with π^+ and π^- at T_π = 140 MeV and $\theta_\pi = 40°$, and at 180 MeV and 30°, 40°, 60°, and 80° using the EPICS system at LAMPF in coincidence with eight plastic scintillators. The inclusive spectra yield cross section ratios $R_\pi = \sigma(\pi^+)/\sigma(\pi^-) = 1.1 \pm 0.1$ at both T_π and all θ_π. Exclusive spectra were obtained between ^{4}He* excitation energies E_x = 21.5 and 45.0 MeV. Angular correlation functions for $(\pi, \pi' p)$ were extracted at T_π = 180 MeV at the four pion angles for selected regions of E_x. The $(\pi^+, \pi^{+'} p)$ angular correlations show a distinct peak near the free proton knockout angle; however, the $(\pi^-, \pi^{-'} p)$ data show either a flat distribution or a minimum near that angle. Calculations, using a distorted wave impulse approximation (DWIA) code which models the $(\pi, \pi' p)$ reaction as a pion-induced proton knockout, predict peaks in the angular correlation functions in the quasifree knockout direction and reproduce quite well the $(\pi^+, \pi^{+'} p)$ data above E_x = 30 MeV. However, these calculations do not resemble the $(\pi^-, \pi^{-'} p)$ data at any excitation energy. Above E_x = 30 MeV, the ratios $R_{\pi p} = \sigma(\pi^+, \pi^{+'} p)/\sigma(\pi^-, \pi^{-'} p)$ were found to be unexpectedly large (up to $R_{\pi p} = 50$) near the free proton knockout angle and very small ($R_{\pi p} = 0.3$) in the opposite direction in contrast to DWIA predictions of 8 and 5, respectively. These discrepancies are evidence that strong interference occurs between the quasifree proton knockout and another process, especially in the $(\pi^-, \pi^{-'} p)$ reaction. Near the ^{4}He $\rightarrow p + t$ breakup threshold, where the 2^-, $T = 0$ state in ^{4}He (E_x = 21.8 MeV) is known to exist, the ratio $R_{\pi p}$ was found to be between 1 and 2 at all pion angles which is in reasonable agreement with the expected value of 1 for the excitation and decay of a state of good isospin.

PACS number(s): 25.80.Hp, 24.30.Cz, 27.10.+h

I. INTRODUCTION

The $(\pi, \pi' p)$ reaction has been used to study the modifications of the pion-nucleon interaction in the nuclear medium. For this purpose, several experiments [1–6] have emphasized measuring $(\pi, \pi' p)$ cross sections at momentum and energy transfers near the values for free pion-proton kinematics. For backward scattered pions (θ_π larger than 90°) the quasifree knockout model of Chant and Roos [7, 8] has been quite successful in explaining the $(\pi^+, \pi^{+'} p)$ data [5, 9].

For the ^{4}He$(\pi^+, \pi^{+'})$ reaction, the kinematic signature of quasifree scattering was seen in the inclusive spectra [10] at a number of incident pion energies and scattered pion angles. A distorted wave impulse approximation (DWIA) calculation, which assumes dominance of quasifree nucleon knockout, reproduced the position of the maxima and the general shape of the spectra at different momentum transfers. By introducing medium modifications using the Δ-hole model, better agreement

*Present address: Rutgers University, Piscataway, NJ 08855.
†Present address: CEBAF, Newport News, VA 23606.
‡Present address: LAMPF, Los Alamos National Laboratory, Los Alamos, NM 87545.
§Permanent address: Lewis and Clark College, Portland, OR 97219.
**Permanent address: University of Pennsylvania, Philadelphia, PA 19104.
††Permanent address: Ben-Gurion University of the Negev, Beer-Sheva, Israel.

with the absolute cross sections was achieved.

In the experiments of Refs. [11–13] ($\pi^{\pm},\pi^{\pm'} p$) triple differential cross sections were measured near particle threshold to gain a better understanding of contributions from unbound nuclear states to the cross sections than is possible from inclusive (π,π') experiments. At selected momentum transfers where the quasifree process is expected to be weak, the excitation of ^{4}He states may be observable. The ^{4}He nucleus has no bound excited states, but broad and overlapping resonances exist in the continuum above particle breakup threshold.

A level diagram of ^{4}He states [14] is presented in Fig. 1. Only states with a significant proton decay width are shown. The threshold energies for proton and neutron emission from ^{4}He* are 19.82 and 20.58 MeV, respectively. The relatively narrow [14, 15] first excited state at 20.2 MeV (0^+, $T = 0$, Γ =0.5 MeV) and the third excited state at 21.8 MeV (2^-, $T = 0$, Γ =2.0 MeV) can be excited by pion scattering, but the excitation of the 0^- state at 21.1 MeV by (π,π') is forbidden by parity conservation. These states have been observed in many different reactions. At higher excitation energies, the resonances are so broad that they form a structureless continuum with each multipolarity having a poorly defined centroid energy and width.

Evidence for the states in ^{4}He near particle breakup threshold in pion inelastic scattering was found in an experiment [16] which measured the ^{4}He($\pi^{\pm},\pi^{\pm'}$) inclusive spectra at $\theta_\pi = 30°$ and $T_\pi = 180$ MeV. Structures in the energy spectra were identified as due to the 0^+, $T = 0$ and 2^-, $T = 0$ states. A ratio $R_\pi = \sigma(\pi^+)/\sigma(\pi^-) = 1.05\pm0.08$ was obtained in Ref. [16] when averaged over excitation energies between 23 and 30 MeV. This value of near unity is expected both for inelastic scattering to states in ^{4}He and quasielastic scattering. Thus, the mechanism exciting the broad continuum could not be determined from the inclusive data. In an attempt to discriminate between the two processes, measurements of the ratio $R_{\pi p}$ of the ^{4}He($\pi^+,\pi^{+'} p$)^{3}H and ^{4}He($\pi^-,\pi^{-'} p$)^{3}H angular correlations were done at two incident energies, 140 and 180 MeV, and several pion scattering angles. The $p + {}^3$H channel was identified by its unique kinematic signature. The 180 MeV data at one pion angle, $\theta_\pi = 30°$, have been reported previously [13]. This paper presents all the data along with a detailed account of their analysis and comparisons with theoretical predictions modeled on a quasifree nucleon knockout mechanism.

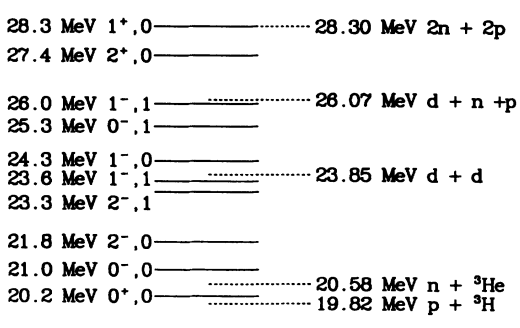

FIG. 1. Level diagram of ^{4}He states [14]. Dashed lines are threshold energies of the designated multiparticle breakups. The solid lines are states in the ^{4}He continuum with the indicated spin-parity and isospin. Most of the resonances are several MeV wide and only the 0^+ state at 20.2 MeV is relatively narrow.

Due to the isospin selectivity of π^+ and π^- scattering, ($\pi,\pi' p$) experiments are sensitive to the reaction mechanism and the isospin structure of the nuclear continuum. Two different values for $R_{\pi p} = \sigma(\pi^+,\pi^+ p)/\sigma(\pi^-,\pi^- p)$ are expected under simple assumptions about the ($\pi,\pi' p$) reaction mechanism. In the quasifree ($\pi,\pi' p$) process, the incident pion interacts with a proton in the target nucleus as if the proton were free. If the ($\pi,\pi' p$) reaction were exclusively quasifree, $R_{\pi p}$ would be near the free π-nucleon elastic cross section ratio of approximately nine at incident energies near the P_{33} π-nucleon resonance. In another possible process which we will call "resonant," the incident pion excites the ^{4}He to an unbound state of unique spin and isospin. Subsequently, the excited ^{4}He decays into any one of a number of different decay channels. This state will decay independently of whether it was excited by π^+ or π^- so that $R_{\pi p} \approx 1$ is expected.

Information on the reaction mechanism can also be obtained from the ^{4}He($\pi,\pi' p$) angular correlation functions. In quasifree scattering, a peak is expected in the angular correlation function, near the direction of the momentum transfer to the target, whereas the decay of a resonant state in ^{4}He would display an angular correlation with a shape according to the quantum numbers of that state. A determination of the relative importance of the quasifree and resonant processes may be possible by studying the ^{4}He($\pi^{\pm},\pi^{\pm'} p$)^{3}H angular correlation function over a wide range of momentum and energy transfer.

II. THE EXPERIMENT

The experiment was conducted at the Los Alamos Clinton P. Anderson Meson Physics Facility (LAMPF) using the Energetic Pion Channel and Spectrometer (EPICS) [17]. At $T_\pi = 180$ MeV, inclusive and exclusive (coincidence) spectra were taken at the four pion angles, $\theta_\pi = 30°$, 40°, 60°, and 80°, and at seven or eight proton angles. At $T_\pi = 140$ MeV data were taken only at $\theta_\pi = 40°$.

In order to detect the outgoing protons, eight plastic scintillators were placed inside a scattering chamber at the angles $\theta_p = -90°$, $-75°$, $-60°$, $-45°$, $-30°$, 90°, 105°, 120°. These angles are measured with respect to the incident beam with positive angles to the left of the beam (the same side as EPICS) and negative angles on the opposite side (Fig. 2). The scintillators were placed at a distance of 63.5 cm from the center of the target, and each scintillator subtended a solid angle of 57 msr. When measurements were done with the spectrometer positioned at $\theta_\pi = 80°$, the scintillator at $\theta_p = 90°$ had to be removed.

The target cell was a cylindrical flask of 12.7 cm diameter with its axis perpendicular to the reaction plane. The walls were made of 25-μm-thick stainless steel, and an aluminum foil heat shield was wrapped around the

flask. The helium gas, in the target cell, was kept at a pressure of $\approx$ 1.5 atm and a temperature of 40 K. This gives a ^{4}He areal density of about 20 mg/cm^2.

The energy loss of the protons in the ^{4}He gas, the target's stainless steel walls, the aluminum around the target and the scintillator wrappings, sets a lower limit on the detectable kinetic energy of the scattered protons. The stainless steel walls and the aluminum have areal densities of 20 and 7 mg/cm^2, respectively. The areal density of the helium gas, 20 mg/cm^2, was chosen as reasonable compromise between the requirements of high counting rate and minimum detectable proton energy. Because of the energy loss in these materials only protons above 5 MeV kinetic energy could be detected. With this lower limit on the proton energy, the accessible ^{4}He excitation energy range started at 21.5 MeV for all pion angles at the negative proton angles. For all positive proton angles the energy loss limited the ^{4}He excitation energy region to above 30 MeV for $\theta_\pi = 30°$ and 40°. Protons did not have enough energy to reach the detectors at positive proton angles for $\theta_\pi = 60°$ and 80°.

The proton events were separated from other charged-particle events using a combination of time-of-flight and pulse-height information from the scintillators. Because the response of plastic scintillators is not a linear function of the energy loss of the charged particles [18], a correction was made to the pulse height. Using the corrected pulse height and the time of flight, a quantity proportional to the particle's mass was calculated. A distinct peak for protons was visible in a histogram of the calculated mass.

With a gate on the proton mass, the two-dimensional

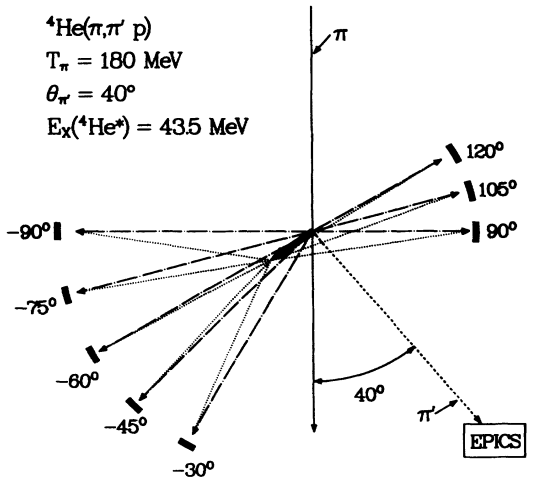

FIG. 2. Diagram of typical laboratory velocity vectors of the ^{4}He$(\pi,\pi'\ p)^3$H reaction. The incident pion (solid line) collides with a stationary ^{4}He nucleus. The scattered pion (dashed line) is detected by EPICS at 40°. The center of mass (c.m.) of the recoiling mass-4 system moves with relatively low velocity (broad solid vector). The laboratory velocity vectors of the protons (chain-dot lines) are the sum of the velocity vectors of the protons in the c.m. system (dotted lines) and the velocity vector of the c.m. system. The angular positions of the scintillators are indicated by the small rectangles.

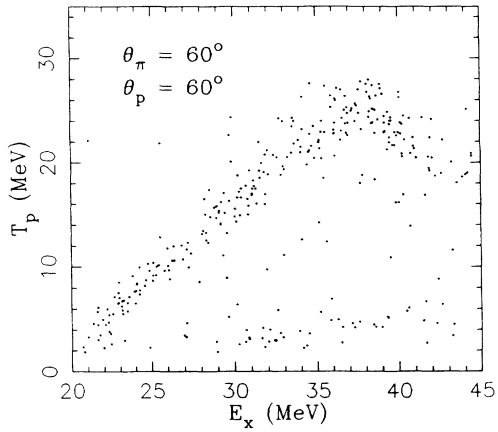

FIG. 3. Two-dimensional histogram of excitation energy E_x in ^{4}He (obtained at $T_\pi = 180$ MeV and $\theta_\pi = 60°$) versus the proton kinetic energy T_p in the proton detector at $\theta_p = -60°$. $T_p = 28$ MeV was the maximum energy of the protons stopped in the scintillator.

histogram of ^{4}He excitation energy versus the proton kinetic energy T_p (Fig. 3) shows a distinctive line for the protons from the p+^{3}H channel. Some events from other possible breakup modes resulting in one or more protons ($p+n+d$, and $p+p+n+n$) can also be seen, but they are weaker and well separated energetically from the p+^{3}H kinematic locus.

The thickness of the scintillators was sufficient to stop protons with kinetic energies up to about 28 MeV. Passing protons create the bend near proton energy of 28 MeV in the p + ^{3}H line as seen in Fig. 3. A two-dimensional gate in the T_p vs E_x plane was placed around the p+^{3}H events (including the protons which passed through the scintillators), and the events were projected on the E_x axis to generate the coincidence spectra for the ^{4}He$(\pi,\pi'p)^3$H reaction.

The absolute cross sections were determined by normalizing measurements of ^{4}He(π,π) elastic yields to a previous experiment [19]. Corrections were made for the momentum dependence of the spectrometer's solid angle. The measured yields were also corrected for chamber efficiency, computer lifetime, and pion decay in flight. An uncertainty of ±5% is estimated for the total correction factor. The target pressure and temperature were measured every two hours and then averaged for each run. The measurement of the target thickness had an uncertainty of ±5%. Thus the uncertainty in the π^+ and π^- cross sections, relative to each other, is 7%, and the error in the ratio of π^+ and π^- cross sections is 10%. The addition of a ±4% error in the absolute normalization [19] leads to an overall uncertainty of about ± 8% in the absolute cross sections.

III. EXPERIMENTAL RESULTS

A. ^{4}He(π,π') inclusive spectra

Background shapes, determined in a previous experiment, were subtracted from the inclusive inelastic pion

spectra and then converted to double-differential cross sections, $d^2\sigma/d\Omega_\pi\, dE_x$ (shown in Fig. 4). Measurements of the ^{4}He(π,π') inclusive cross sections near particle threshold were made previously [16] at $T_\pi = 180$ MeV and $\theta_\pi = 30°$. Distorted wave impulse approximation (DWIA) calculations of the ^{4}He(π,π') inclusive energy spectra were done using wave functions from the recoil corrected continuum shell model (RCCSM) [20] for the 0^+, 2^-, 1^-, and 2^+ multipolarities. The calculated contributions from each multipolarity were added together for comparison with the experimental spectra, and good agreement was found. Though the predicted energy spectra for each of the multipolarities generally are very broad, different regions of the energy spectra are dominated by a particular multipolarity.

In Ref. [16] the transitions to the 0^+ state at $E_x = 20.2$ MeV and the 2^- state at $E_x = 21.8$ MeV could be identified. A small shoulder just above particle threshold was seen at $\theta_\pi = 30°$ and reproduced by the RCCSM calculation [20] for the 0^+ multipolarity which includes a narrow peak near 20.2 MeV (see Fig. 1 in Ref. [16]). This shoulder is also seen in the present data at $\theta_\pi = 30°$ and 40°, though not as clearly as in Ref. [16]. The 2^- multipolarity includes the 2^- resonance state at 21.8 MeV which appeared as a peak near that energy in both the experiment and the predictions in Ref. [16]. The cross section for the 2^- state at 21.8 MeV is expected to peak at $\theta_\pi = 60°$ [21]. In the present data, the spectra at all angles have a small peak near 22 MeV, and the peak is most pronounced at 60°.

According to the RCCSM, which includes resonant and quasifree scattering in a consistent way, the 1^- multipolarity (which includes the giant dipole resonance) is largest in the region between 23 and 30 MeV in ^{4}He and the 2^+ multipolarity (which includes the giant quadrupole resonance) is largest in the region above 30 MeV [16]. At $T_\pi = 180$ MeV, the peak in the angular distribution of a 1^- excitation is expected near $\theta_\pi = 40°$ [21].

In the previous experiment [16], which measured ^{4}He($\pi^\pm,\pi^{\pm\prime}$) inclusive data, $R_\pi = \sigma(\pi^+)/\sigma(\pi^-) = 1.05 \pm 0.08$ at $\theta_\pi = 30°$ was determined when the cross sections were averaged over the excitation energy region between 23 and 30 MeV. From the present data $R_\pi = 1.1 \pm 0.10$ was extracted at 30° and 40° in agreement with the earlier work. $R_\pi = 1.1 \pm 0.10$ was measured also at 60° and 80°. Hayes [22] predicted $R_\pi = 1.08$ at $\theta_\pi = 30°$ and $R_\pi = 1.57$ at $\theta_\pi = 50°$ with DWIA calculations using a simple two-state mixing model and the isospin mixing amplitude from Ref. [23]. The constant R_π measured in this experiment at all angles suggests that the isospin mixing amplitude of Ref. [23] is too large.

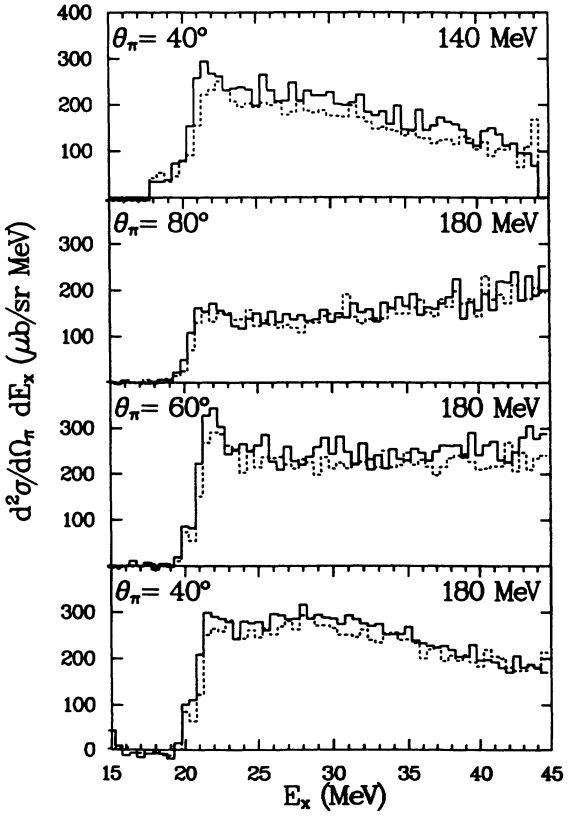

FIG. 4. Inclusive pion inelastic cross sections as a function of ^{4}He excitation energy E_x at $T_\pi = 180$ MeV and $\theta_\pi = 40°$, 60°, 80° and at $T_\pi = 140$ MeV and $\theta_\pi = 40°$. The π^+ (π^-) spectra are the solid (dashed) histograms.

B. ^{4}He(π,π' p) exclusive data

1. ^{4}He(π,π' p) spectra

The ^{4}He(π,π' p)^{3}H triple differential cross sections $d^3\sigma/d\Omega_\pi\, d\Omega_p\, dE_x$, at $T_\pi = 180$ MeV and $\theta_\pi = 30°$, 40°, 60°, and 80° are shown in Figs. 5 and 6. The exclusive cross sections in the figures were averaged over the five proton detectors located at the negative (forward) angles. The statistical errors are typically 15%. The exclusive energy spectrum at $T_\pi = 140$ MeV and $\theta_\pi = 40°$ (not shown) is similar to those at 180 MeV. Certain features in the excitation energy spectra, expected for excitation of states in ^{4}He or for quasifree scattering, will now be discussed.

In the naive quasifree knockout picture, the residual nucleus is treated as a spectator and the pion is assumed to interact only with a single nucleon. In this case, the maximum of the quasifree cross section in the pion energy spectra will be at an energy

$$\Delta T_\pi = q^2/2M \qquad (1)$$

below the incident energy. Here q is the momentum transfer in a free pion-nucleon collision and M is the mass of the nucleon [24]. For $\theta_\pi = 30°$, 40°, 60°, and 80° at $T_\pi = 180$ MeV, ΔT_π corresponds to ^{4}He excitation energies of 8, 14, 28, and 42 MeV, respectively. For $\theta_\pi = 30°$ and 40°, these predicted excitation energies of the cross section maxima are below the particle breakup threshold ($E_x = 19.82$ MeV). Because of the Fermi momentum distribution of the nucleons in the target nucleus, however, quasifree events are expected above the particle breakup threshold.

In the (exclusive) excitation energy spectra measured with π^+, the cross sections were found to peak around 28, 31, and 45 MeV for $\theta_\pi = 30°$, 40°, and 60°, respectively, and the π^+ energy spectrum at 80° suggests a peak above 45 MeV. In order to obtain predictions for the *shape* of the energy spectra in the quasifree model, one must account for the momentum distribution of the nucleons in the nucleus, the distortion of the incident pion wave by the target nucleus, and the distortion of the scattered pion and proton waves by the residual nucleus. Such a calculation was done by us using the DWIA model of Chant and Roos [7] (see Sec. IV).

The shape of the measured π^- energy spectra is very different from that of the π^+ spectra. At all pion angles a distinctive peak appears in the π^- spectra near 22 MeV. If this peak were caused by the detection threshold cutting into the quasielastic continuum, then $R_{\pi p}$ should be approximately the quasifree value of nine. Instead, $R_{\pi p}$ in this region of excitation is between 1 and 2 at all pion angles. The π^- (inclusive) cross section near 22 MeV has a maximum at $\theta_\pi = 60°$. These two features indicate that the peak is primarily due to the excitation of the 2^- state centered at $E_x = 21.8$ MeV. It could not be the 0^+, $T = 0$ state at 20.2 MeV, because protons from its decay have energies below the proton detection threshold. In the π^+ spectra at $\theta_\pi = 30°$ and 40°, the yield from the quasifree scattering dominates the spectra and obscures the peak from the 2^- state that is seen in the π^- spectrum. But at $\theta_\pi = 60°$ and 80°, the peak in the quasifree cross section has moved to higher excitation energies so that the peak from the 2^- state can be observed in the π^+ spectra as well.

Between $E_x = 25$ and 35 MeV, the giant resonance region, a surprisingly large ratio, $R_{\pi p} = 15$ to 20, is found for these spectra which were averaged over the forward proton angles. (Even larger ratios are observed for individual proton angles. See below.) The large observed ratios are in disagreement with both the assumption of excitation and decay of an excited state in ^{4}He and the assumption of a simple quasifree knockout process. At

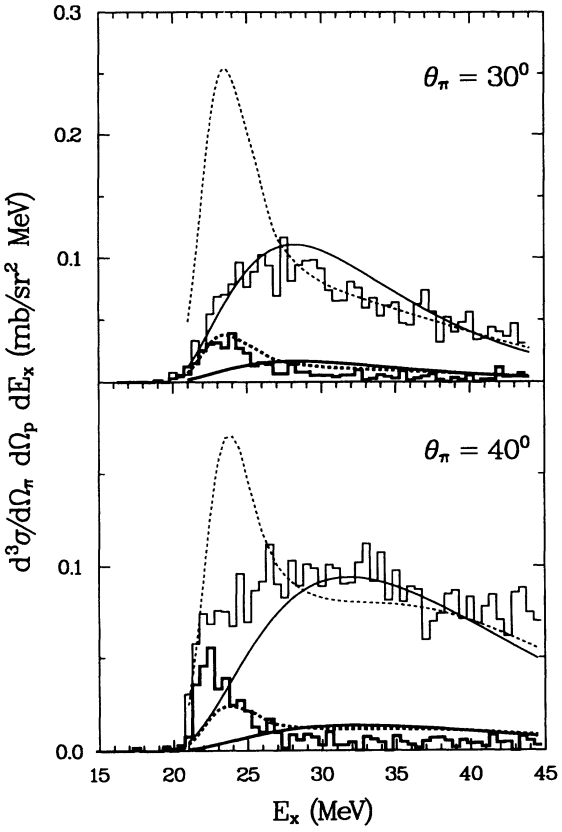

FIG. 5. Exclusive ^{4}He$(\pi^\pm, \pi^{\pm'} p)^3$H excitation energy spectra (or triple differential cross sections) measured at $T_\pi = 180$ MeV and $\theta_\pi = 30°$ and 40°. The π^+ (π^-) data and calculations are the thin (thick) solid and dashed curves. The cross sections have been averaged over the five proton detectors at negative angles. The solid (dashed) curves are the results of DWIA calculations using the π + nucleus fit A and the energy-independent (energy-dependent) $p + t$ optical potential.

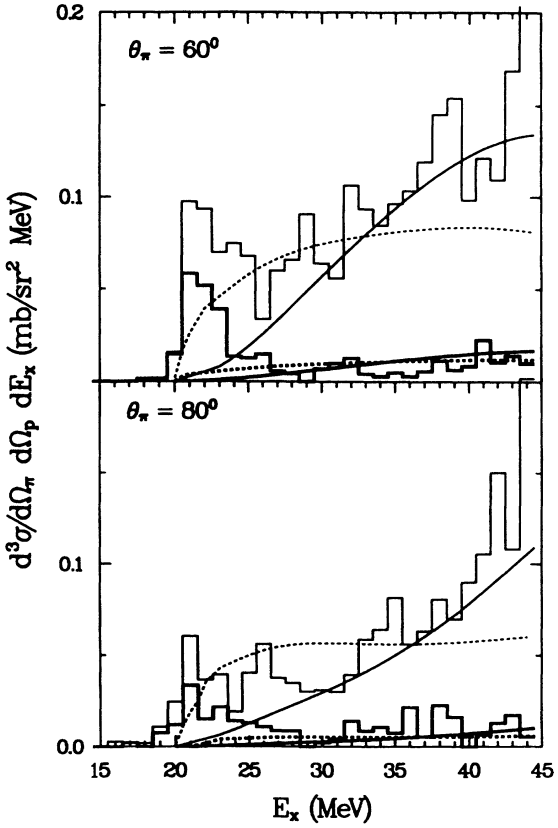

FIG. 6. Exclusive ^{4}He$(\pi^\pm, \pi^{\pm'} p)^3$H excitation energy spectra measured at $T_\pi = 180$ MeV and $\theta_\pi = 60°$ and 80°. The π^+ (π^-) data and calculations are the thin (thick) solid and dashed lines. The solid (dashed) lines are results of DWIA calculations using the π + nucleus fit A (fit B) and the energy-independent $p + t$ optical potential. The solid lines are the DWIA results multiplied by the factor 2.5 at $\theta_\pi = 60°$ and 4.0 at 80° in order to fit the π^+ data at high excitation energies. The dashed lines are DWIA calculations without such a factor.

higher excitation energies, $E_x \geq 40$ MeV, $R_{\pi p}$ decreases with increasing pion angle and, at $\theta_\pi = 80°$, $R_{\pi p}$ is near or below the value of about 9 expected (in the plane wave impulse approximation) for quasifree scattering.

2. ^{4}*He*(π,π' *p*) *angular correlation functions*

The angular correlation functions, or double differential cross sections $d^2\sigma/d\Omega_\pi\, d\Omega_p$, were created by summing the yields over ^{4}He excitation energy regions of a few MeV at each proton angle. Guided by the inclusive spectra [16, 22] predicted by the RCCSM, the total measured region of E_x, from 21.5 to 45 MeV, was divided into four parts: $21.5<E_x<25.0$, $25.0<E_x<30.0$, $30.0<E_x<40.0$, and $40.0<E_x<45.0$ MeV (see Sec. IV B 2). The double-differential cross sections in the center-of-mass system of the recoiling mass-4 system and the cross section ratios are shown as a function of the proton angle $\theta_p^{\text{c.m.}}$ for the four regions of excitation energy in Figs. 7–10. In these figures, $\theta_p^{\text{c.m.}}$ is the angle between the velocity vector of the mass-4 c.m. system (thick arrow in Fig. 2) and the velocity vector of the proton in the mass-4 c.m. system (dotted arrow in Fig. 2) with positive proton angles in the counterclockwise direction.

The double-differential cross sections in the laboratory frame were transformed by the appropriate Jacobian into the center of mass of the recoiling mass-4 (c.m.) system to obtain the $d^2\sigma/d\Omega_\pi\, d\Omega_p$. Each excitation energy has a slightly different angular transformation. The $d^2\sigma/d\Omega_\pi\, d\Omega_p$ were plotted at the average of the proton angles $\theta_p^{\text{c.m.}}$ in the c.m. system for each excitation energy region (Figs. 7–10).

At $\theta_\pi = 30°$ and 40°, the protons could be detected in all eight detectors when the ^{4}He excitation energy was greater than 30 MeV. This was possible because the kinetic energy of the protons was sufficient to overcome the energy loss in the ^{4}He gas and the walls of the target can.

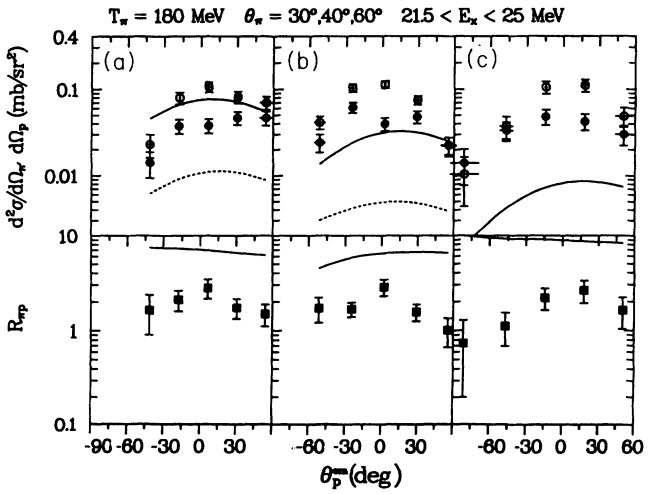

FIG. 7. Top: Angular correlation functions for ^{4}He($\pi,\pi'p$) at (a) $\theta_\pi = 30°$, (b) 40°, and (c) 60°, summed over $21.5<E_x<25.0$ MeV (π^+, open circles; π^-, closed circles). The solid (dashed) lines are DWIA predictions for π^+ (π^-) assuming quasifree proton knockout using fit A for the π-nucleus optical potential and the energy-independent proton-triton optical potential. For $\theta_\pi = 60°$ the DWIA predictions were multiplied by 2.5. Bottom: The ratio $R_{\pi p} = \sigma(\pi^+,\pi^{+\prime}p)/\sigma(\pi^-,\pi^{-\prime}p)$ of the double differential cross sections plotted in the top of the figure. The solid line is $R_{\pi p}$ from the DWIA predictions plotted in the top.

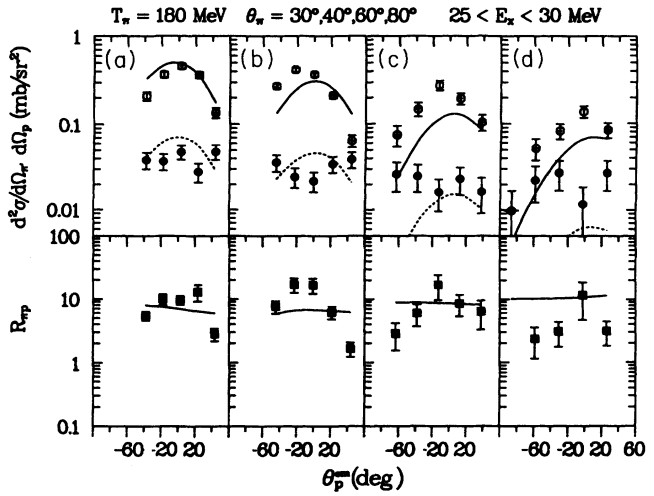

FIG. 8. Top: Angular correlation functions for ^{4}He($\pi,\pi'p$) at (a) $\theta_\pi = 30°$, (b) 40°, (c) 60°, and (d) 80°, summed over $25<E_x<30.0$ MeV. Description of lines and labels is given in Fig. 7. For $\theta_\pi = 60°$ and 80° the DWIA predictions were multiplied by 2.5 and 4.0, respectively. Bottom: The ratio $R_{\pi p}$ of the double differential cross sections plotted in the top of the figure. The solid line is $R_{\pi p}$ from the DWIA predictions plotted in the top.

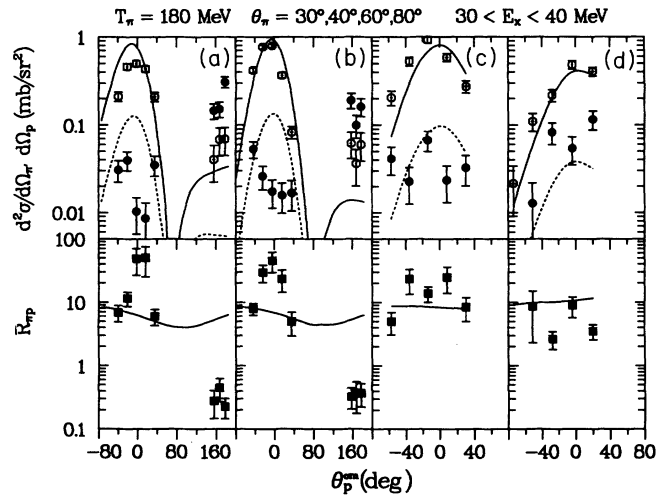

FIG. 9. Top: Angular correlation functions for ^{4}He($\pi,\pi'p$) at (a) $\theta_\pi = 30°$, (b) 40°, (c) 60°, and (d) 80°, summed over $30<E_x<40$ MeV. Description of lines and labels is given in Fig. 7. For $\theta_\pi = 60°$ and 80° the DWIA predictions were multiplied by 2.5 and 4.0, respectively. Bottom: The ratio $R_{\pi p}$ of the double differential cross sections plotted in the top of the figure. The solid line is $R_{\pi p}$ from the DWIA predictions plotted in the top.

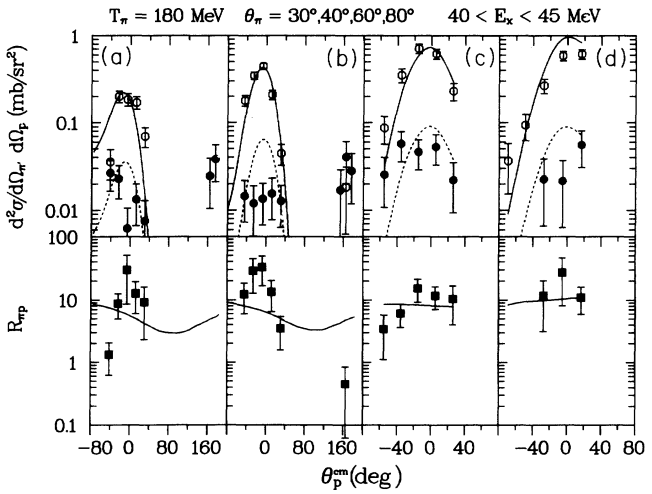

FIG. 10. Top: Angular correlation functions for ^{4}He$(\pi,\pi' p)$ at (a) $\theta_\pi = 30°$, (b) 40°, (c) 60°, and (d) 80°, summed over $40<E_x<45$ MeV. For $\theta_\pi = 60°$ and 80° the DWIA predictions were multiplied by 2.5 and 4.0, respectively. Description of lines and labels is given in Fig. 7. Bottom: The ratio $R_{\pi p}$ of the double differential cross sections plotted in the top of the figure. The solid line is $R_{\pi p}$ from the DWIA predictions plotted in the top.

Thus, the $(\pi,\pi p)$ angular correlation functions include a few points at $\theta_p^{\text{c.m.}}$ near 180°.

In the quasifree knockout picture, the peak in the angular correlation is expected in the direction of the momentum transfer to the recoiling ^{4}He, that is, $\theta_p^{\text{c.m.}} = 0°$. We emphasize that for E_x above 30 MeV, the π^+ angular correlations indeed show a distinct peak at the quasifree knockout angle in sharp contrast to the π^- angular correlations. Thus the data of this work suggest that quasifree knockout plays a dominant role in the $(\pi^+,\pi^{+'}\, p)$ but probably not in the $(\pi^-,\pi^{-'}\, p)$ reaction. This was verified by DWIA calculations with the code THREEDEE [7, 8] which fit only the π^+ data in the quasifree recoil direction. These calculations will be discussed in some detail in the next section.

IV. ANALYSIS OF THE DATA

A. Quasifree knockout calculations

1. Introduction

In this section we present a brief summary of the description of the program THREEDEE as given in Ref. [8]. We also discuss the application of this program to ^{4}He$(\pi,\pi'\, p)^3$H.

THREEDEE treats the $A(\pi,\pi'\, p)B$ reaction as a pion-induced quasifree proton knockout in the framework of the impulse approximation (IA). In this model, the transition operator is replaced by the two-body π-p operator. An additional approximation is made in the factorized IA, i.e., the arguments of the two-body t matrix are replaced by their asymptotic values. This approximation is valid if the t matrix varies slowly with energy. In the factorization approximation the t matrix squared becomes a multiplicative factor which can be expressed by the two-body π-p half-off-the-energy-shell cross section $(d\sigma/d\Omega)_{\pi p}$. With these approximations, the triple differential cross section can be written as [Eq. (6) in Ref.[8]]:

$$\frac{d^3\sigma}{d\Omega_\pi d\Omega_p dE_\pi} = KC^2 S_{l,j} \left(\frac{d\sigma}{d\Omega}\right)_{\pi p} \sum_\lambda |\, T_{BA}^{\alpha l\lambda}\,|^2 \qquad (2)$$

where K is a product of kinematic factors. C^2 is the square of an isospin Clebsch-Gordan coefficient and $S_{l,j}$ is the spectroscopic factor as defined by Kurath [25].

$T_{BA}^{\alpha l\lambda}$ is the distorted wave matrix element:

$$T_{BA}^{\alpha l\lambda} = \frac{1}{\sqrt{2l+1}} \int \chi_{\pi B}^{(-)^*}(\mathbf{k}_{\pi B},\mathbf{r})\chi_{pB}^{(-)^*}(\mathbf{k}_{pB},\mathbf{r}) \times \chi_{\pi A}^{(+)}(\mathbf{k}_{\pi A},\gamma\mathbf{r})\phi_{l\lambda}^{\alpha}(\mathbf{r})d^3r, \qquad (3)$$

where the χ's are the distorted waves for the incident pion/target-nucleus system (πA), the outgoing pion/residual-nucleus system (πB), and the knocked-out proton/residual-nucleus system (pB). $\mathbf{k}_{\pi A}$, $\mathbf{k}_{\pi B}$, and $\mathbf{k}_{pB}$ are the relative momenta for the particle pairs indicated by the subscripts. $\gamma = B/(B+1)$ where B is the mass (in u) of the residual nucleus. $\phi_{l\lambda}^{\alpha}$ is the bound single nucleon wave function determined from the overlap of the residual nucleus and the proton. We took $\phi_{l\lambda}^{\alpha}$ from Greben's parametrization of the nucleon-trinucleon overlap function in ^{4}He which includes meson exchange effects [26]. $C^2S_{l,j} = 2$ was used for the knock-out of a $1s$-shell proton from ^{4}He according to the naive shell model.

In THREEDEE, the half-off-the-energy-shell π-p cross section is approximated by the on-shell π-p cross section. Because the π-p center-of-mass energies are different in the incident and outgoing channels, an ambiguity exists in determining at which π-p relative center-of-mass energy to calculate the on-shell cross section. In the calculations presented in this paper, the final energy prescription was employed which uses the π-p relative asymptotic energy after the collision. The π-p cross sections were calculated from the phase shifts of Rowe *et al.* [27].

2. Pion-nucleus optical potentials

The pion-nucleus distorted waves were obtained by solving the Klein-Gordon equation using the Kisslinger optical potential [28]

$$U = -A\{b_0\, p_\pi^2\, \rho(r) + b_1 \bigtriangledown \cdot [\rho(r)\bigtriangledown]\} \qquad (4)$$

where A is the number of target nucleons, b_0 is the complex s-wave parameter, b_1 is the complex p-wave parameter, $\rho(r)$ is the nuclear density, and p_π is the incident pion momentum. The parameters b_0 and b_1 can be calculated from the π-nucleon phase shifts [27]. They may also be treated as free parameters to improve the fit to elastic scattering data. For the incident pion energies

TABLE I. The b_0 and b_1 parameters following the prescription of Ref. [29] (C–H) and the fitted parameters.

	Re b_0	Im b_0	Re b_1	Im b_1
C–H	−0.5231	0.2682	3.6940	6.5378
Fit A	−0.6000	5.0000	0.7000	12.000
Fit B	−1.7000	0.3000	3.7000	15.000

of this experiment, where the $P_{3,3}$ resonance dominates the π-p reaction, the Kisslinger potential is known to work well for nuclei between ^{12}C and ^{208}Pb, only if the b_0 and b_1 parameters are obtained from the π-p phase shifts at an energy ≈30 MeV below the incident pion energy [29]. However, for the present work on ^{4}He(π,π) at T_π = 180 MeV the use of energy-shifted b_0 and b_1 parameters (first row in Table I) did not fit the elastic data satisfactorily. The calculation (dashed line in Fig. 11) reproduces the minimum at the correct angle; however, at forward and backward angles the data disagree strongly with the calculations. One possible reason that the calculations using the energy-shifted b_0 and b_1 parameters in Eq. (4) do not produce good fits to the data is that the $(A-1)/A$ factor from the Kerman-McManus-Thaler formalism [30] is not used. This omission should be partly compensated for by fitting the b_0 and b_1 parameters to the data.

Calculations, done with b_0 and b_1 determined with another or no energy shift, did not improve the fit to the data. Therefore we treated b_0 and b_1 as fitting parameters. Two equivalent fits to the elastic data were found with the parameter sets called fit A and fit B (Table I). The elastic cross sections calculated with the fit A and fit B parameters are shown in Fig. 11 as solid and dotted lines, respectively. In the region of momentum transfer where the (π,π' p) data were taken ($\theta_{\rm lab} \leq 80°$), the fits are quite good, although the quality of the fit at larger angles is not satisfactory. The effect of using different sets of fit parameters on the predicted (π,π' p) triple differential cross sections will be discussed below. For all calculations shown here, the same b_0 and b_1 were used in creating the incident and outgoing π-nucleus distorted waves.

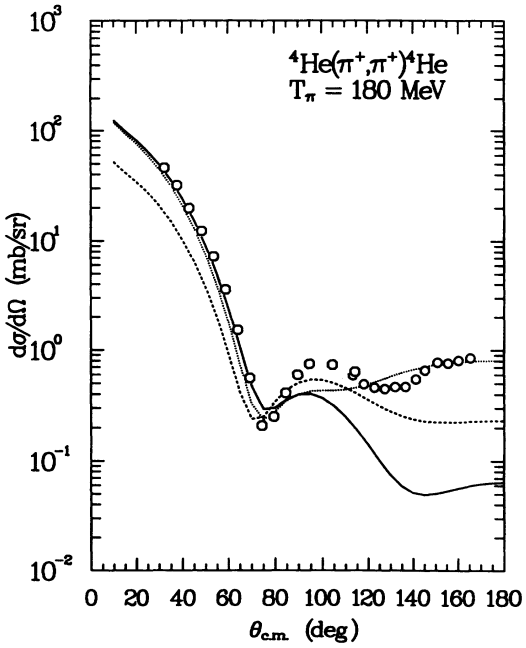

FIG. 11. ^{4}He(π^+,π^+) elastic scattering data [19] at T_π = 180 MeV and calculations using a Kisslinger potential with different b_0 and b_1 parameters. Dashed line: b_0 and b_1 determined from the π-nucleon phase shifts of Ref. [27] with an energy shift of 28 MeV; solid line: fit A; dotted line: fit B (see Table I).

3. *Proton–triton optical potential*

The proton-triton distorted waves were generated using the complex Woods-Saxon optical potential of the form:

$$V_{\rm opt}(r) = -\frac{V_0}{1+e^{\left(\frac{r-r_0 A^{1/3}}{a_0}\right)}} - \frac{iW_i}{1+e^{\left(\frac{r-r_i A^{1/3}}{a_i}\right)}}. \quad (5)$$

The optical potential parameters were taken from a fit by Podmore and Sherif [31] to ^{3}He(p,p) elastic scattering data over an incident proton energy range of 5 to 50 MeV. In the fit of Ref. [31] the geometry parameters were kept constant, whereas the depth parameters were varied at each proton energy. The geometry parameters are

$$r_0 = 1.488\,\text{fm},\ a_0 = 0.144\,\text{fm},$$
$$r_i = 1.501\,\text{fm},\ a_i = 0.378\,\text{fm}.$$

The real and imaginary depth parameters of Ref. [31] are listed in Table II. We have fitted a second-order polynomial in proton energy T_p to the depth parameters. The polynomials are

$$V_0(\text{MeV}) = 53.82 - 0.8577T_p + 0.00265T_p^2,$$
$$W_i(\text{MeV}) = -0.510 + 0.115T_p + 0.0031T_p^2.$$

We modified THREEDEE so that the depth parameters were calculated from the polynomial for the scattered proton energy (in the p + ^{3}He laboratory system).

Ideally, the optical parameters from a fit to ^{3}H(p,p) [not ^{3}He(p,p)] elastic scattering should be used in the calculation. But ^{3}H(p,p) elastic scattering data exist only in a limited energy region, and no optical model fit to the data was found in the literature. In order to find out whether the optical potential parameters which reproduced p + ^{3}He data are very different from those for p + ^{3}H, we fitted the p + ^{3}H data of Ref. [32] at T_p = 13.6, 16.2, and 19.5 MeV using the optical model search code RELOM [33]. The fitted optical parameters were not substantially different from the parameters for p + ^{3}He scattering of Ref. [31]. Some change in the parameters is expected, since a difference exists between the p+^{3}He and the p+^{3}H interactions. (For p+^{3}H elastic scattering the T = 1 and T = 0 parts of the nuclear force are involved in the interaction, whereas p+^{3}He in-

TABLE II. The real V_0 and imaginary W_i well depths (in MeV) of the p + ^{3}He optical potential of Ref. [31] as a function of incident proton energy (in MeV).

T_p	5.51	6.82	8.82	10.8	13.6	16.2	19.4	30.0	49.5
V_0	50.25	48.26	46.63	44.61	41.63	38.99	38.33	32.30	17.44
W_i	0.00	0.00	1.20	1.37	1.18	0.94	3.55	6.05	12.64

teracts only by the $T = 1$ part of the force.) Apparently, the large observed differences between the p + ^{3}H and p + ^{3}He experimental cross sections are mainly due to the Coulomb force.

B. Comparison with experimental data

1. *Excitation energy spectra*

The experimental π^+ and π^- triple differential cross sections, $d^3\sigma/d\Omega_\pi\, d\Omega_p\, dE_x$, and the results from the DWIA calculations with THREEDEE for the ^{4}He$(\pi, \pi'\, p)^3$H reaction at $T_\pi = 180$ MeV and $\theta_\pi = 30°$ and 40°, are shown in Fig. 5. For comparison with the (angle-averaged) experimental exclusive spectra, the calculations were averaged over the five proton detector angles of $\theta_p = -90°$, $-75°$, $-60°$, $-45°$, and $-30°$ as a function of ^{4}He excitation energy at each pion scattering angle.

The dashed lines in Fig. 5 are the results of calculations using the fit A parameters for the pion-nucleus optical potential and the parameters with the energy-dependent depths for the proton-triton optical potential. In the region of excitation energy below 26 MeV, the real depth in the proton-triton optical potential [31] is about 50 MeV. At all pion angles, these calculations exhibit a large bump centered near $E_x = 24$ MeV which is not present in the π^+ data. However, there is a peak at about 1 to 2 MeV below that energy in the π^- data which we identified as due to the excitations of the 2^- state at 21.8 MeV and not due to quasifree scattering.

The solid lines in Fig. 5 are the results of the DWIA calculations with the same pion-nucleus optical potential as for the dashed line, but the real and imaginary depth parameters for the proton-triton optical potential were fixed at 32 and 6 MeV, respectively, over the entire range of ^{4}He excitation energy. With the lower real depth in the proton-triton optical potential near breakup threshold, the strong (resonant) enhancement at $E_x \approx$ 24 MeV has disappeared and the fit to the exclusive π^+ spectra is much better. Changing the imaginary depth parameter had little effect on the calculations for $E_x \leq$ 26.0 MeV. Regardless of which proton-triton potential was used, above $E_x = 25$ MeV the π^+ calculations agree with the data, but the predictions for π^- are larger than the data by a factor of at least two.

The effect that the energy-dependent proton-triton optical potential causes an enhancement in the ^{4}He$(\pi^+, \pi^+\, p)$ calculated cross sections near particle threshold has been reported in Ref. [10] which also used the optical potential parameters of Ref. [31]. It was noted that this (spin-independent) optical potential produces a resonance in the $l = 1$ partial wave. This potential resonance contains states of spin and parity $J^\pi = 2^-, 1^-$, and 0^- with $S = 1$ and $J^\pi = 1^-$ with $S = 0$ where S is the p + t channel spin. [As noted before, the 0^- state cannot be reached by ^{4}He(π, π').] If spin-dependent terms were included in the DWIA calculations, these potential resonance states would split resulting in a broadening of the potential resonance peak. Another problem in using an optical potential for calculations near the breakup threshold (i.e., at proton energies below 5 MeV in the p +^{3}H laboratory system) is the fact that the optical model may not be reliable at these low energies.

The experimental excitation energy spectra and the DWIA calculations of this work at $\theta_\pi = 60°$ and 80° are shown in Fig. 6. As in Fig. 5, the solid line was obtained using fit A parameters for the pion-nucleus optical potential and the energy-independent proton-triton optical potential. Above $E_x = 26$ MeV, the π^+ calculations with fit A parameters reproduce the shape of the 60° and 80° spectra, but the calculated cross section had to be multiplied by 2.5 and 4.0, respectively, to agree with the magnitude. With the same multiplicative factors, the π^- calculations predict too large cross sections at 60°, but the predictions agree qualitatively with the π^- data at 80°.

A broad quasifree bump is predicted to peak near 46 MeV in the π^+ calculations at $\theta_\pi = 60°$ and the data and calculations appear to show the lower E_x half of this quasifree peak. The calculation at $\theta_\pi = 80°$ (solid line) matches the shape of the measured excitation energy spectrum and shows that the centroid of the quasifree peak has moved above the experimental range with only its tail appearing in the spectra.

The effects on the predicted cross section of changing the pion-nucleus optical model have also been studied. Calculations (dashed line in Fig. 6) that used the b_0 and b_1 parameters of fit B in the π-nucleus potential and the energy-independent p-t optical potential did not need to be multiplied by any factor to match the magnitude of the measured cross sections. The same increase in predicted cross section occurs at $\theta_\pi = 30°$ and 40° and makes the agreement at these angles with the absolute cross sections using fit A appear fortuitous. Also the shape of the predicted excitation energy spectrum is changed when the parameters in the π nucleus changed. The strong dependence of the absolute cross section on the pion optical parameters cancels almost completely in the calculated ratio $R_{\pi p}$. Use of different pion-nucleus optical potentials yield $R_{\pi p}$ which differ by less than 10%.

2. *Angular correlation functions*

The calculated angular correlations were summed over four regions of excitation energy at each pion angle for comparison with the data (Figs. 7–10). The calculations were done with fit A parameters for the pion-nucleus optical potential and the energy-independent proton-triton optical potential. The calculated cross sections at $\theta_\pi = 60°$ and 80° have been multiplied by 2.5 and 4.0, respectively. Since the magnitude of the calculations is strongly dependent on the input parameters for the pion distorted waves, the following discussion will focus on the quality of the fit to the general shape and the position of the maxima in the angular correlation functions and on the ratio $R_{\pi p} = \sigma(\pi^+,\pi^{+\prime}p)\ /\sigma(\pi^-,\pi^{-\prime}p)$ which are reasonably independent of the input parameters.

As mentioned above (Sec. III B 2), guided by the RCCSM prediction of the inclusive spectra (Refs. [16, 22]), the four regions of excitation energy were chosen in order to emphasize different multipolarities in the ^{4}He continuum. The first region is from 21.5 to 25.0 MeV where the 2^-, $T = 0$ state is located. The second region is from 25.0 to 30.0 MeV where the 1^- multipolarity is expected to dominate, but a tail from the 2^- multipolarity is also present. The third region is from 30 to 40 MeV where the 2^+ multipolarity is predicted to be strong, but the 1^- multipolarity is still present. The fourth region of E_x extends from 40 to 45 MeV. Contributions from the quasifree process are expected to be large in different regions of E_x, depending on the momentum transfer. Between 40 and 45 MeV in E_x the quasifree process is expected to dominate at the large pion angles, $\theta_\pi = 60°$ and 80°.

In the $21.5 < E_x < 25$ MeV region (Fig. 7) the experimental data give $R_{\pi p} \approx 2$ at all pion angles. The DWIA calculation with the energy-dependent proton-triton optical potential predicts a peak at $E_x = 24$ MeV and $R_{\pi p} \approx 7$. Calculations performed with the real depth parameter fixed at 32 MeV (which eliminates the peak at $E_x = 24$ MeV) also predict $R_{\pi p} \approx 7$. The near equality of the experimental π^+ and π^- cross sections indicates that a state of good isospin is excited in this excitation energy region and that quasifree scattering is relatively unimportant. The state of good isospin is the 2^-, $T = 0$ state centered at $E_x = 21.8$ MeV.

At all pion angles and at excitation energies above $E_x = 25$ MeV (Figs. 8–10), the π^+ calculations and data peak at nearly the same proton angle, $\theta_p^{\text{c.m.}} \approx 0$. The predicted shape and width of this peak are in good agreement with the π^+ data. However, the π^- calculations and data disagree strongly. Where peaks in the angular correlation are predicted, the data are constant or display a minimum.

At $\theta_\pi = 30°$ and 40° and above $E_x = 25$ MeV, the calculations predict $R_{\pi p}$ between 5 and 8. The measured $R_{\pi p}$ is nearly 50 at the quasifree angle in the region of $30 < E_x < 40$ MeV (Fig. 9). Above $E_x = 40$ MeV, the measured $R_{\pi p}$ drops to between 15 to 30 (Fig. 10).

Surprisingly, for $\theta_\pi = 30°$ and 40°, the π^- cross section near $\theta_p^{\text{c.m.}} = 180°$ is larger than the cross section at the quasifree proton knockout angle $\theta_p^{\text{c.m.}} = 0°$. The measured $R_{\pi p}$ is ≈ 0.3 whereas the predicted $R_{\pi p}$ for proton knockout is ≈ 5. This inversion in $R_{\pi p}$ from the predicted value is indicative of interference between two processes. The possibility of triton knockout being responsible for this inversion is discussed in a forthcoming publication [39].

In the region of $25 < E_x < 30$ MeV, the transition to the GDR is expected to be strong at $\theta_\pi = 30°$ and 40°. If this region were excited only by the transition to the GDR ($T = 1$), we would expect the ratio $R_{\pi p}$ to be one, but the measured $R_{\pi p}$ is between 10 and 20. Though the ratio is not as large as at the higher excitation energies, it is still about twice as large as the ratio predicted for pure quasifree scattering.

At $\theta_\pi = 60°$, the DWIA with fit A and the energy-independent p-t optical potential, predicts the position of the maximum in the cross section at about $E_x = 46$ MeV and a half-width of the quasifree bump of about 25 MeV. In the $30 < E_x < 40$ MeV region, the measured $R_{\pi p}$ is near 20 at the peak of the angular correlation. This value of $R_{\pi p}$ is lower than at $\theta_\pi = 30°$ and 40°, but it is still larger than the predicted value. The decrease in $R_{\pi p}$ with higher momentum transfer indicates that the quasifree amplitude becomes more dominant. Indeed, at $\theta_\pi = 80°$ and above $E_x = 25$ MeV, the measured $R_{\pi p}$ are at or even below the predicted values. At this angle the π^- data are usually above the predicted values when the π^+ calculations are normalized to the data. At this high momentum transfer one may expect [6] contributions from processes involving multiparticle emission which might decrease $R_{\pi p}$ below the expected quasifree ratio.

V. RELATED EXPERIMENTS

Phenomena similar to the ones observed in this work have been seen in other experiments. ^{12}C($\pi,\pi'p$) and ^{208}Pb($\pi,\pi'n$) experiments [11, 12] have studied nuclear structure near particle emission threshold. Angular correlation functions for ^{12}C($\pi,\pi'p$) were measured at $T_\pi = 180$ MeV and $\theta_\pi = 20°$. This pion angle is near the peak of the angular distribution for the giant dipole resonance [34].

The experiment on ^{12}C measured $R_{\pi p} = 3.09 \pm 0.62$ at the quasifree angle and $R_{\pi p} = 0.47 \pm 0.11$ at 180°, i.e., in the opposite direction in the ^{12}C center-of-mass system. As in the present work, the quasifree knockout code THREEDEE [7, 8] was used in the analysis. It predicted a nearly angle-independent $R_{\pi p} = 7.4$ and fitted the $(\pi^+,\pi^{+\prime}\ p)$ data reasonably well, but the $(\pi^-,\pi^{-\prime}\ p)$ predictions were below the data. Also, the measured angular dependence of $R_{\pi p}$ disagrees with the angle independent value of 1.0 that is expected from the excitation and decay of the giant dipole resonance. This leads to the hypothesis that constructive interference between the quasifree and resonant processes could explain the angular dependence of $R_{\pi p}$.

Large cross section ratios have been observed in the work on the ^{16}O($\pi,\pi'p$)^{15}N(g.s.) reaction at $T_\pi = 240$ MeV [4]. These authors have studied the

$(\pi, \pi'\ p)$ reaction specifically under quasifree kinematic conditions. Emitted protons of high kinetic energy ($T_p \geq 35$ MeV) were detected at the quasifree angle for $\theta_\pi = 35°$, 60°, 130°. $R_{\pi p} \approx 40$ was observed at $\theta_\pi = 35°$. As the pion angle was increased to 130°, the ratio decreased to the quasifree ratio.

Kyle *et al.* have interpreted the large ratio as due to an interference between direct pion-induced quasifree proton knockout and knockout of a proton by the intermediate Δ formed by the π-nucleon interaction (Δ-N knockout). Using the Δ-hole formalism [35], the amplitude for Δ knockout of a proton was estimated to be similar in magnitude but opposite in sign to the amplitude for direct π^--induced proton knockout. In contrast, the Δ-N knockout is relatively unimportant for the $(\pi^+, \pi^{+'}\ p)$ reaction which is dominated by the direct π^+-induced proton knockout. Extensive Δ-hole calculations presented in Ref. [36] have reproduced the $^{16}O(\pi, \pi' p)$ data only qualitatively. One major difference between the ^{16}O experiment and the present work is that the former experiment looked explicitly at high excitation energies where no ^{16}O states are expected. The data of this paper should provide a test of reaction models in the region of the nuclear continuum where states are known to exist.

Triple differential cross sections for $^3He(\pi^\pm,\pi^{\pm'}p)$ have been measured [6] at $T_\pi = 220$ and 270 MeV for $\theta_p = -43°$ and θ_π between 45° and 120°. $R_{\pi p} = 5.5 \pm 0.8$ was observed at $\theta_\pi = 75°$ and $T_\pi = 220$ MeV, whereas calculations using THREEDEE predicted $R_{\pi p} = 8.6$. All other experimental values of $R_{\pi p}$ were near or below the prediction. The authors of Ref. [6] postulated that multiparticle scattering was responsible for the experimental ratio being below the quasifree values. Similar behavior has been seen in the present work for ^4He at $\theta_\pi = 80°$ in the continuum above 25 MeV.

At present no Δ-hole calculations are available for the $^4He(\pi, \pi'\ p)^3H$ reaction. As mentioned in the introduction, measurements were made of inclusive inelastic $^4He(\pi^+,\pi^{+'})$ cross sections at various incident energies near 180 MeV [10]. These data exhibited features of quasifree scattering and were well explained by Δ-hole calculations. We note that interference effects would not be exhibited by the inclusive data.

The general features of quasifree nucleon knockout were seen in the $^4He(\pi^+, \pi^{+'}p)^3H$ and $^4He(\pi^+, \pi^{+'}n)^3He$ experiments by Balestra *et al.* [37] using nuclear emulsions. Plane wave impulse approximation calculation by Mach *et al.* [38] disagreed with the shape of the pion angular distributions and the measured ratio of $(\pi^+, \pi^{+'}\ p)$ to $(\pi^+, \pi^{+'}\ n)$ total cross sections. By adding a term representing the knockout of ^3He or ^3H the predicted shape of the pion angular distribution was in better agreement with experiment, but disagreement between the calculated and measured ratios of the total cross sections persisted. In attempts to interpret our data, the three-nucleon knockout model would be a natural way to explain the observation of $R_{\pi p} < 1$ at backward proton angles, but it would not explain the large values of $R_{\pi p}$ at the quasifree proton knockout angle. (See Ref. [39].)

VI. SUMMARY

The data of this work have provided strong evidence for the dominance of the quasifree knockout mechanism in the $(\pi^+, \pi^{+'}\ p)$ reaction on ^4He in the region of excitation energy of the giant dipole and quadrupole resonances and beyond. This conclusion was drawn from the measured positions and widths of the peak in the measured angular correlation functions. A different story emerged from the π^- data. The shape of the π^- angular correlation functions often show a minimum near the quasifree knockout angle which suggests destructive interference between the quasifree amplitude and at least one other amplitude.

Evidence was found for excitation and decay of a nuclear state in the ^4He continuum near particle breakup threshold. In the region of $21.5 \leq E_x \leq 25.0$ MeV, the inclusive spectra show a definite peak which is most pronounced at 60° . In this region $R_{\pi p}$ was found to be ≈ 2 at θ_π between 30° and 80°. Unlike at higher excitation energies, this ratio is near the value of one which is expected for a process involving the formation and decay of a state of good isospin. Thus, a large fraction of the yield in this region of excitation energy is probably due to the 2^-, $T = 0$ state centered at $E_x = 21.8$ MeV.

Above $E_x = 25$ MeV, the measured ratios at the quasifree angle are much larger than the calculated values for quasifree scattering, $R_{\pi p} \approx 7$. Specifically in the region $30 < E_x < 40$ MeV, values of $R_{\pi p}$ as large as ≈ 50 were found. The discrepancy between the experiment and the prediction of the quasifree model is evidence for interference between quasifree scattering and another process. The interference is apparently destructive for π^- near the quasifree angle.

A model which predicts destructive interference at the quasifree knockout angle, is the Δ-N knockout model [35]. Calculations of angular correlation functions from this model would thus be useful to test its validity for $^4He(\pi, \pi'\ p)$.

The giant dipole and quadrupole resonances can be excited in the region $30 < E_x < 40$ MeV. The amplitude for excitation of the GDR is expected to peak near $\theta_\pi = 40°$ and $R_{\pi p} \approx 1$ is expected. However, at this pion angle the largest values of $R_{\pi p}$ were measured. Calculations of the angular correlation functions with a model, such as the RCCSM which treats quasifree and resonance scattering in a consistent way, are needed to interpret the data.

ACKNOWLEDGMENTS

This work was supported in part by the U. S. Department of Energy and the Robert A. Welch Foundation. We thank Dr. N. S. Chant for permission to use the THREEDEE code, and Dr. M. Khandaker for help in its use. We also thank Mr. L. Atencio for his help in constructing and operating the cryogenic target.

[1] H. J. Ziock, R. J. Ellis, K. O. H. Ziock, J. Bolger, E. Boschitz, J. Arvieux, R. Corfu, and J. Piffaretti, Phys. Rev. Lett. **43**, 1919 (1979).
[2] H. J. Ziock, R. J. Ellis, K. O. H. Ziock, J. Bolger, E. Boschitz, J. Arvieux, R. Corfu, and J. Piffaretti, Phys. Rev. C **24**, 2674 (1981).
[3] E. Piasetzky *et al.*, Phys. Rev. Lett. **46**, 1271 (1981); Phys. Rev. C **25**, 2687 (1982).
[4] G. S. Kyle, P.-A. Amandruz, Th. S. Bauer, J. J. Domingo, C. H. Q. Ingram, J. Jansen, D. Renker, J. Zichy, R. Stamminger, and F. Volger, Phys. Rev. Lett. **52**, 974 (1984).
[5] J. R. Hurd, J. S. Boswell, R. C. Minehart, L. B. Rees, Y. Tzeng, H. J. Ziock, and K. O. H. Ziock, Nucl. Phys. **A462**, 605 (1987).
[6] A. Klein, J. P. Egger, C. Gysin, R. Henneck, J. Jourdan, M. Pickar, G. R. Plattner, and I. Sick, Nucl. Phys. **A472**, 605 (1987).
[7] N. S. Chant and P. G. Roos, Phys. Rev. C **15**, 57 (1977).
[8] L. Rees, N. S. Chant, and P. G. Roos, Phys. Rev. C **26**, 1580 (1982).
[9] N. S. Chant, L. Rees, and P. G. Roos, Phys. Rev. Lett. **48**, 1784 (1982).
[10] M. Baumgartner, H. P. Gubler, G. R. Plattner, W. D. Ramsay, H. W. Roser, I. Sick, P. Zupranski, J. P. Egger, and M. Thies, Nucl. Phys. **A399**, 451 (1983).
[11] S. H. Yoo *et al.*, Phys. Rev. Lett. **63**, 738 (1989).
[12] S. H. Yoo *et al.*, J. Phys. G **16**, L89 (1990).
[13] M. K. Jones *et al.*, Phys. Rev. C **42**, R807 (1990).
[14] D. R. Tilley, H. R. Weller, and G.M. Hale, Nucl. Phys. A (to be published).
[15] T. Walcher, Phys. Lett. **31B**, 442 (1970).
[16] C. L. Blilie *et al.*, Phys. Rev. Lett. **57**, 543 (1986).
[17] H. A. Thiessen and S. Sobottka, Los Alamos Scientific Laboratory Report No. LA-4534-MS, 1978 (unpublished).
[18] C. R. Craun and D. L. Smith, Nucl. Instrum. Methods **80**, 239 (1970).
[19] B. Brinkmöller *et al.*, Phys. Rev. C **44**, 2031 (1991).
[20] D. Halderson and R. J. Philpott, Nucl. Phys. **A221**, 295 (1979).
[21] C. L. Blilie, Ph.D. thesis, University of Minnesota, 1985 (unpublished).
[22] A. C. Hayes, Phys. Rev. C **39**, 699 (1989).
[23] F. C. Barker, Aust. J. Phys. **37**, 583 (1984).
[24] T. Ericson and W. Weise, *Pions and Nuclei* (Clarendon Press, Oxford, 1988), p. 255.
[25] D. Kurath, Phys. Rev. C **7**, 139 (1973).
[26] J. M. Greben, Phys. Lett. **111B**, 363 (1982).
[27] G. Rowe, M. Salomon, and R. H. Landau, Phys. Rev. C **18**, 584 (1978).
[28] L. S. Kisslinger, Phys. Rev. **98**, 761 (1955).
[29] W. B. Cottingame and D. B. Holtkamp, Phys. Rev. Lett. **45**, 1828 (1980).
[30] A. Kerman, H. McManus, and R. Thaler, Ann. Phys. (N.Y.) **8**, 551 (1959).
[31] B. S. Podmore and H. Sherif, in *Few Body Problems in Nuclear and Particle Physics*, edited by R. J. Slobodrian, B. Cujec, and K. Ramavataram (Les Presses de l'Univesite Lavel, Quebec, 1975), p. 517.
[32] J. L. Detch *et al.*, Phys. Rev. C **4**, 52 (1971).
[33] M. A. Franey, computer code RELOM, based on computer code RAROMP by G. J. Pyle (unpublished).
[34] L. C. Bland, Ph.D. thesis, University of Pennsylvania, 1984 (unpublished); Los Alamos National Laboratory Report No. LA-9960-T, 1984 (unpublished).
[35] M. Hirata, F. Lenz, and M. Thies, Phys. Rev. C **28**, 785 (1983).
[36] T. Takaki and M. Thies, Phys. Rev. C **38**, 2230 (1988).
[37] F. Balestra, L. Busso, R. Garfagnini, G. Piragino, R. Barbini, C. Gauraldo, and R. Scrimalio, Lett. Nuovo Cimento **15**, 535 (1976).
[38] R. Mach, M. G. Sapozhnikov, R. Scrimalio, C. Gauraldo, F. Balestra, R. Garfagnini, and G. Piragino, Nuovo Cimento **45A**, 325 (1978).
[39] J. L. Langenbrunner *et al.* (unpublished).